On molecular recognition of an uranyl chelate by monoclonal antibodies

Jean-marie Teulon, Michael Odorico, Shu-wen Chen, Pierre Parot, Jean-luc Pellequer

JOURNAL OF MOLECULAR RECOGNITION
J. Mol. Recognit. 2007; **20**: 508–515
Published online in Wiley InterScience
(www.interscience.wiley.com) DOI:10.1002/jmr.854

On molecular recognition of an uranyl chelate by monoclonal antibodies†

Jean-Marie Teulon[1], Michael Odorico[1], Shu-wen W. Chen[2], Pierre Parot[1] and Jean-Luc Pellequer[1]*

[1]CEA VALRHO, DSV/iBEB/SBTN, BP 17171, 30207 Bagnols sur Cèze, France
[2]13 Avenue de la Mayre, 30200 Bagnols sur Cèze, France

The energy landscape of the uranyl (UO_2) chelate dissociated from a monoclonal antibody U08S was investigated using dynamic force spectroscopy (DFS). The uranyl ion (UO_2^{2+}) is chelated with the ligand dicarboxy-phenanthroline (DCP). The monoclonal antibody U08S was raised against UO_2–DCP and does not cross-react with DCP alone. The results of plotting the most probable force against the logarithm of the loading rate show two distinguished values of slopes of multiple fitting lines, as observed in our previous study on that system with monoclonal antibody U04S (Odorico *et al*., 2007a. Biophys. J. 93: 645–654.). It indicates an unbinding process undergoing at least two activation states. We have generated the histogram of unbinding events with respect to the composite stiffness of the complex between the protein and the uranyl compound. Combining the model of Bell and Evans with that of Williams, we have estimated the number of parallel bonds involved in the unbinding process and determined the value of stiffness for individual bonds. We propose that the uranyl compound binds to the two antibodies U04S and U0c at structurally equivalent locations and forms the interaction with similar coordination modes. In addition, the unbinding process goes through two steps; the first weakens the bonding of the central metal with AspL50 of the antibody and the second breaks other non-bonded interactions of the compound with the antibody.

Keywords: **antibody–metal interaction; single molecules; chelated UO_2; protein–ligand interactions; transition state theory; kinetic dissociation rate; atomic force microscopy; actinides**

Received 23 July 2007; revised 9 August 2007; accepted 16 August 2007

INTRODUCTION

Environmental toxicology aims at determining chemical and radiological toxic effects of elements used in nuclear research and industry. To establish human and environmental heavy metal toxicity thresholds, it is important to characterize the interactions between biological targets (e.g., proteins or DNA) and the soluble form of metals including actinides (Gorden *et al*., 2003). The uranyl ion (UO_2^{2+}) is the most common species encountered in aqueous solutions of uranium (Ansoborlo *et al*., 2006; Pible *et al*., 2006) and is known to become incorporated in bones and tissues (Vidaud *et al*., 2005). In the study of tracing uranium chemicals in the body, we chose a model system where the uranyl ion can be specifically recognized by monoclonal antibodies. We obtained several monoclonal antibodies (Mabs) raised against uranyl–dicarboxy-phenanthroline (UO_2–DCP) compounds and selected the ones for their high UO_2–DCP specificity. In a previous study (Odorico *et al*., 2007a), we have used Mab U04S and characterized its binding interaction with the uranyl-chelate compound by dynamic force spectroscopy (DFS) (Evans and Ritchie, 1997; Evans, 2001). We have characterized the energy landscape of UO_2–DCP unbinding from Mab U04S and have shown that the unbinding process occurs through at least two energy barriers where the inner one has a width less than 1 Å and the outer barrier greater than 1 Å. The results of measured unbinding forces have allowed us to build two structurally different molecular models for UO_2–DCP binding to either of two accessible aspartic acids in the binding site of Mab U04S. The presence of multiple parallel bonds involved in this receptor–ligand interaction complicates the evaluation of dissociation rate constants for the unbinding process which were found to vary between 0.06 and 13.2 s^{-1}.

To gain more insight into molecular interactions of UO_2–DCP with antibody, we have used Mab U08S, another monoclonal antibody with a slightly different sequence from Mab U04S, for further investigating the influence of the protein environment on the binding strength. As before, we used the atomic force microscopy (AFM) technique and analyzed DFS for rupture forces of unbinding between Mab U08S and UO_2–DCP in order to characterize the kinetic behavior of [UO_2–DCP]–Mab U08S dissociation.

*Correspondence to: J.-L. Pellequer, CEA VALRHO, DSV/iBEB/SBTN, BP 17171, 30207 Bagnols sur Cèze, France. E-mail: jean-luc.pellequer@cea.fr
†J.-M. Teulon and M. Odorico contributed equally to this work.

Abbreviations: Mab, monoclonal antibody; Fab, antibody fragment; AFM, atomic force microscopy; DFS, dynamic force spectroscopy; DCP, 2,9-dicarboxy-1,10-phenanthroline.

AFM has many advantages for kinetic studies of slow dissociation processes occurring over weeks or months in natural condition (e.g., avidin–biotin system). In DFS, the activation energy of the process is lowered by applying an external force to pull the ligand away from the protein and this makes it possible to determine a wide range of non-covalent binding strengths. The importance of accurate determination of intermolecular binding strength in environmental toxicology lies in its application for the rational design of appropriate reagents that bind toxic materials with desired affinity as well as specificity. The use of DFS for this purpose can avoid many-particle interference on determining the relevant interaction parameters in bulk solutions.

MATERIALS & METHODS

Instrumental setups

A dimension 3100 AFM microscope with a Nanoscope IV controller (Digital Instrument Veeco, Santa Barbara, CA, USA) was used for measuring unbinding forces of the molecular system. The experiments were carried out using the force mode of AFM that produces force–displacement curves. We independently determined the spring constants of all the gold-coated tips used (Olympus Biolever, Olympus—Veeco NPG), as previously described (Odorico *et al*., 2007b). Calibration of a new mounted tip was routinely performed after every chemical treatment during the course of an AFM experiment using the thermal noise method. We calculated standard error deviations of cantilever spring constants to be around 10–25% for soft tips (<10 pN/nm) and 7–15% for stiff tips (>10 pN/nm). We obtained a wide range of loading rates by controlling either the retracting speed of the piezo scanner or the spring constant of the cantilever using a linear speed and an opened loop. The applied loading rate r_e was calculated as the product of the scan rate v and the slope of the force–displacement curve just before the record of a rupture event. The slope, k_{eq}, is a quantity describing a composite elastic property of the cantilever tip with the interacting molecules under study. The elastic effect of the molecules of interest is represented by stiffness k_p that is obtained from the equation $1/k_{eq} = 1/k_c + 1/k_p$, where k_c is the spring constant of the cantilever. Concerning the contact between tip and sample, we set the delay at 0; the contact time was calculated for each case. For instance, with a retraction speed of 82 nm/s and a spring constant of 4.9 pN/nm, the average calculated contact time is 2s.

Molecular systems

Since the results of our previous study on Mab U04S indicated no specific interaction with UO_2–DCP in systems 3 (UO_2–DCP chelate on the tip while the substrate lacks the antibody Mab U04S) and 4 (only DCP compound attached on the tip through a PEG spacer, protein A-Mab U04S on the substrate saturated with BSA) (Odorico *et al*., 2007a), we only used two experimental setups for Mab U08S that are respectively analogous to systems 1 and 2 for Mab U04S. In the first, the UO_2–DCP compound was attached on the tip with protein A-Mab U08S on the substrate slide saturated with BSA. In the second, the metal-free chelate DCP was attached on the tip keeping the same substrate. The procedure of functionalization of tips and gold-coated glass slides was as described previously (Odorico *et al*., 2007a).

Kinetic analysis

According to Bell's model (Bell, 1978) that was further developed by Evans (Evans and Ritchie, 1997), hereafter called Bell–Evans model, the force distribution of unbinding events, $P_B(F)$,can be described as follows:

$$P_B(F) = (k_d(0)/r)\exp\{F/f_\beta + (k_d(0)f_\beta/r)[1-\exp(F/f_\beta)]\}$$

where the force normalization factor is $f_\beta = \frac{k_B T}{\gamma}$, k_B is the Boltzmann constant, T is the temperature, γ is the energy barrier width from the stable to activated state, and $k_d(0)$ is the dissociation rate constant at zero force. Consequently, the most probable unbinding force F^* can be written as

$$F^* = f_\beta \ln(r) - f_\beta \ln[k_d(0)f_\beta]$$

As mentioned earlier, r_e is the applied loading rate. In an ideal case, the unbinding event occurs between a single pair

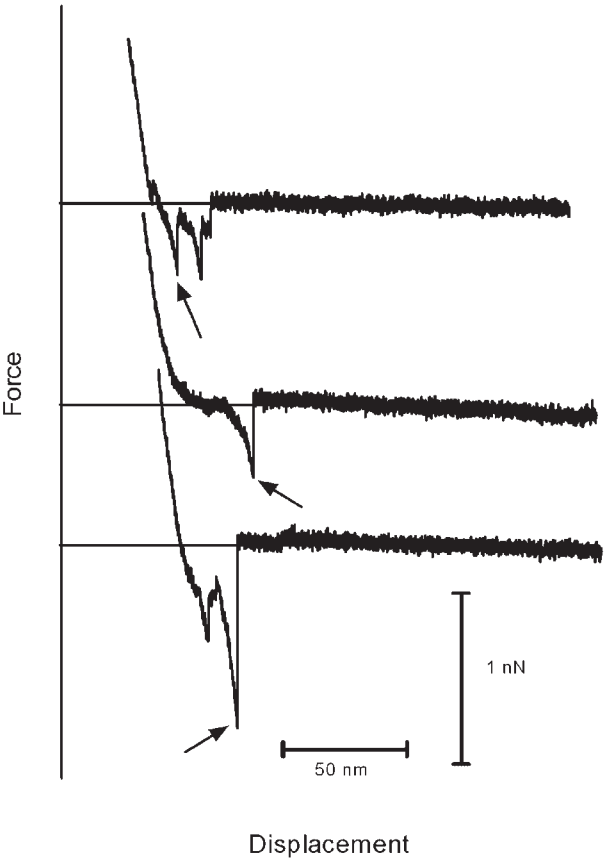

Figure 1. Representative experimental force–displacement curves. The force (*Y*-axis) is represented in nN while the displacement (*X*-axis) is represented in nm. Selected rupture peaks are indicated by black arrows. The majority of measured curves correspond to those with a single rupture event (middle curve).

DOI: 10.1002/jmr

of molecules and goes through only one activation state; the plot of F^* vs. $\ln(r_e)$ can then be fitted with a straight line so that the value of γ can be obtained from the slope, and $k_d(0)$ from the intercept with the force coordinate axis. However, when the unbinding event involves rupture of parallel bonds with an unknown number n, the composite protein stiffness is $k_p = n\ k_{p1}$, where k_{p1} characterizes stiffness of a single bond, an intrinsic property (Erdmann, 2005). To obtain the loading rate for multiple parallel-bond systems, we adopted the Williams formalism (Evans and Williams, 2002; Williams, 2003); data analysis based on this formalism will be referred to as the Williams model:

$$r_f = k_0 \frac{k_B T}{\gamma} \left[\sum_{n=1}^{N} \frac{1}{n^2} \exp\left(-\frac{F^* \gamma}{n k_B T} \right) \right]^{-1}$$

Three-dimensional model of Mab U08S

The variable region of Mab U08S has been sequenced. A comparative modeling technique was used to build a three-dimensional model of the recombinant variable fragment of Mab U08S (Pellequer *et al*., 2000; Pellequer *et al*., 2005). Due to the strong similarity between Mab U04S and Mab U08S, the same antibody template was used (PDB code 1AY1) (Murali *et al*., 1998). The sequence identity was about 88% without insertions or deletions. Side chains were replaced, optimized (Chen and Pellequer, 2004), and refined by a computational graphic procedure. All atomic positions were energy minimized using X-PLOR (Brünger, 1992) with the CHARMM22 force field parameters (MacKerell *et al*., 1998). The model quality was evaluated by PROCHECK (Laskowski *et al*., 1993) with 82.5% of ϕ, ψ dihedral angles in the most favorable regions. The CDRH3 loop was remodeled as made for model B in Mab U04S (Odorico *et al*., 2007a). The 3-D structure of the UO_2–DCP was obtained as previously described (Odorico *et al*., 2007a).

RESULTS AND DISCUSSIONS

Distribution of the most probable unbinding forces

We have selected 1527 force–displacement curves (Figure 1) where 1382 unbinding events were used for data analysis corresponding to 20–30% of collected experiments. The applied loading rates were clustered into several bins where each bin contains 100 events and the values of loading rates ranged from 134 to 133 252 pN/s. The smallest one in the Mab U08S system is markedly larger than that in Mab U04S (Odorico *et al*., 2007a). An empirical distribution of unbinding forces is plotted in Figure 2.

To characterize non-specific interactions in the measurements for the Mab U08S system, we compared the results between experimental setups with and without the uranyl ion on the tip. The results show detectable non-specific interactions in about 10% of the experiments. A histogram of non-specific unbinding events at a loading rate of 1808 pN/s ($\ln = 7.5$) is displayed in Figure 3. We note an overlap between non-specific and specific unbinding events

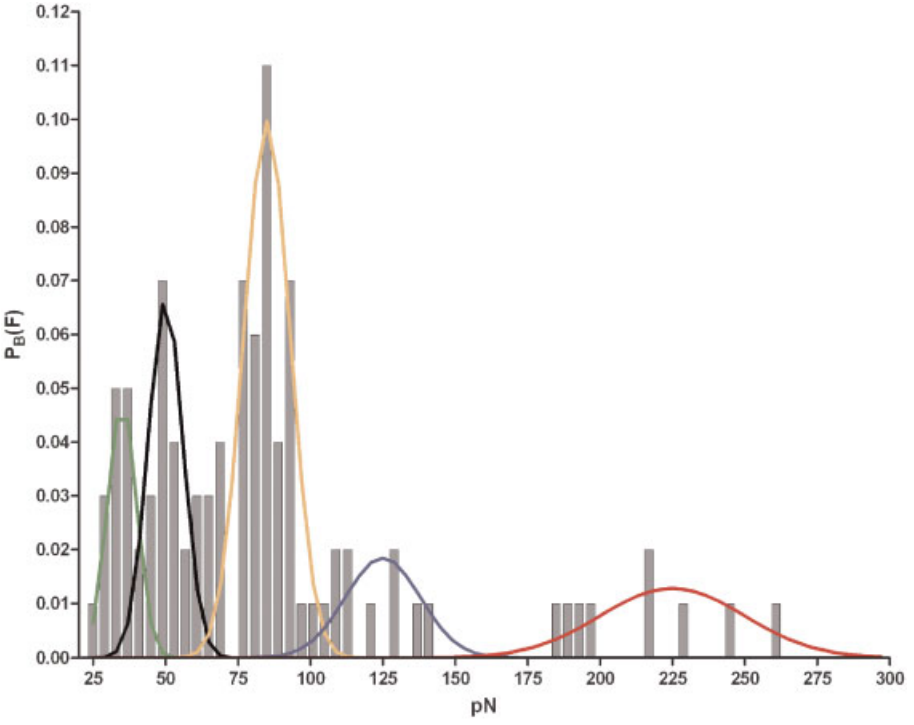

Figure 2. The histogram of unbinding events of UO_2–DCP complexed with Mab U08S at the loading rate $r_e = 972$ pN/s. The force bin size is 5 pN. The histogram was fitted with Gaussian distribution functions, as described previously (Odorico *et al.*, 2007b). The maximum of each Gaussian curve corresponds to the most probable unbinding forces F^*. This figure is available in colour online at www.interscience.wiley.com/journal/jmr

DOI: 10.1002/jmr

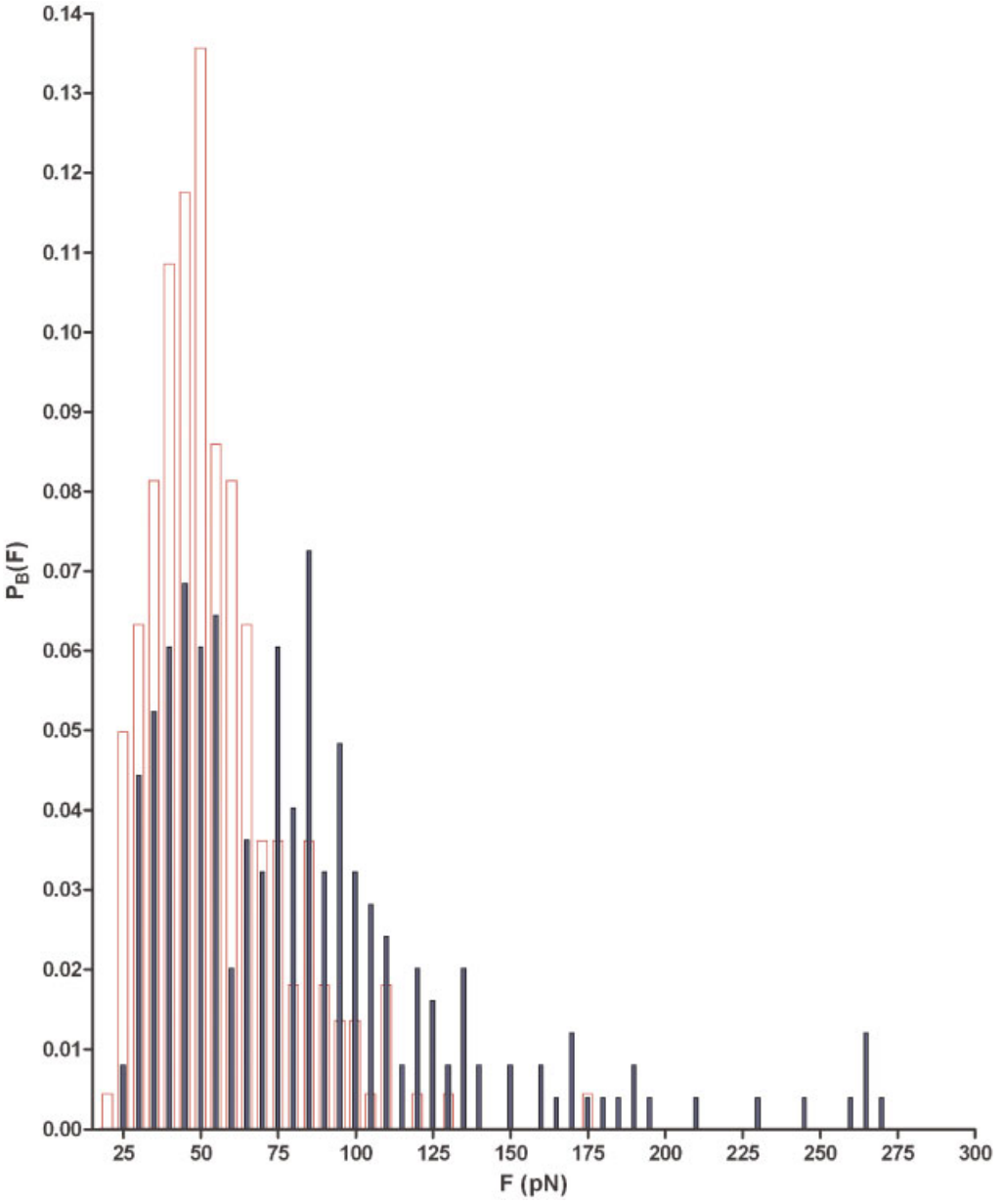

Figure 3. The force distributions of unbinding events with respect to non-specific interactions (opened bars, without UO_2^{2+} on the tip) and specific interactions in the presence of UO_2^{2+} (filled bars). The corresponding loading rates were 1998 and 1808 pN/s with an optimized force bin size of 5 pN. This figure is available in colour online at www.interscience.wiley.com/journal/jmr

in the presence of the uranyl ion (Figure 3). This strong overlap of the first peak in histograms is characteristic of the presence of non-specific interactions, as observed in the Mab U04S system. For subsequent peaks, only moderate or no overlapping exists between non-specific and specific unbinding events.

Kinetics analysis for multiple parallel bonding systems

By modeling the most probable rupture forces with a linear function of the logarithm of measured loading rates, the multiplicity of bonding involved in the unbinding process requires multiple regression lines (Figure 4). As observed in the Mab U04S system, the unbinding process for the Mab U08S system also displays two slopes where the transition occurs in a loading rate region between 1096 and 8103 pN/s.

In this study, we used a concentration for Mab U08S lower than for Mab U04S, leading to a concomitant reduction in the number of parallel regression lines. We obtained five and seven linear fits, respectively at low and high loading rates for the Mab U08S system.

To analyze DFS data for a system undergoing multiple activation processes, one linear relation between F^* and $\ln(r_e)$ is no longer valid (Odorico *et al*., 2007a). If the system is further complicated by the presence of multiple parallel

DOI: 10.1002/jmr

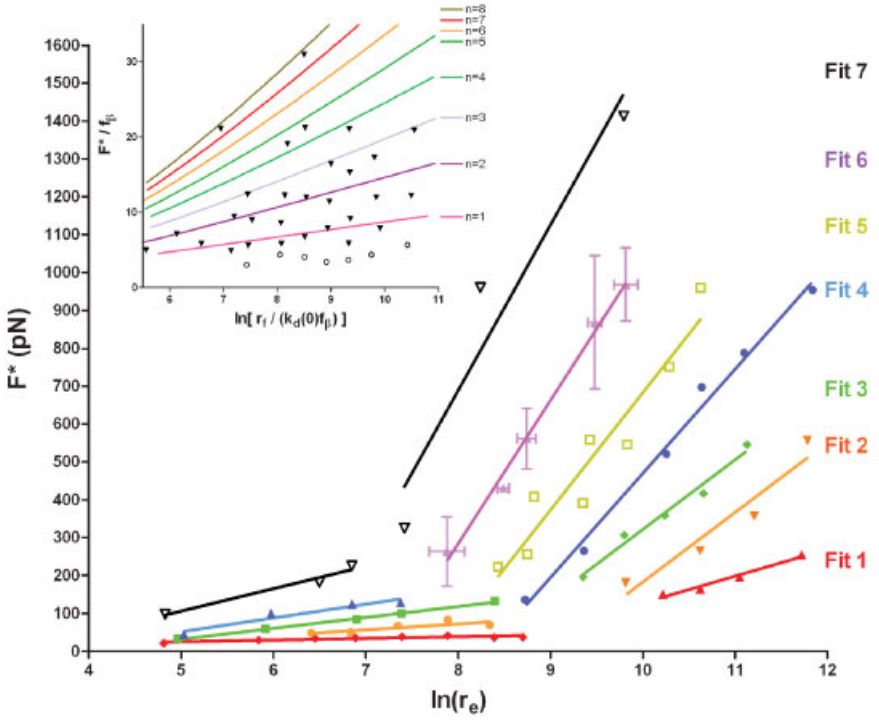

Figure 4. The plot of F^* vs. $\ln(r_e)$ shows analysis results based on the Bell–Evans model for UO_2–DCP unbinding from Mab U08S. Five and seven fits are made in the regions of low and high loading rates, respectively. For clarity, only fits at high loading rates are labeled and standard deviations are only indicated for fit 6. Inset shows the results according to the Williams model using $\gamma = 0.09$ nm and $k_d(0) = 0.08\,s^{-1}$.

bonds, the simple Bell's model is obviously not sufficient for modeling the data (Evans and Williams, 2002; Williams, 2003). We therefore used the Williams model (Williams, 2003) to obtain the relationship between the unbinding force of n parallel bonds and the corresponding loading rate through an ensemble of bonding states of the system. This theory has been successfully applied to the Mab U04S system (Odorico *et al.*, 2007a) and others (Sulchek *et al.*, 2005). As presented in the inset of Figure 4, the fittings revealed the presence of up to eight bonds at high loading rate, though single to triple parallel bonds are most populated. Note that one antibody contains two antigen binding fragments (Fabs). Very interestingly, we found that non-specific unbinding events do not fit any category of parallel bonds using the Williams model (labeled by opened circles in Figure 4). The presence of multiple parallel bonds is explained by the fact that the cantilever is entirely coated with ligand molecules (UO_2–DCP) and that about 1000 antibodies/μm^2 are coated on the flat substrate. Although experiments are performed without stopping the tips near the surface, the contact time is in the order of a second. Consequently, our system is well adapted to analyze unbinding events of multiple parallel bonds. It should be remembered that antibodies, through their two Fabs, naturally bind antigens using parallel bonds.

The energy barrier width γ and the dissociation rate constant $k_d(0)$ for UO_2–DCP unbinding from Mab U08S are listed in Table 1. Each set of parameters corresponds to one regression line in Figure 4. Using the Williams model, several data points could not be fitted at both low and high

Table 1. The calculated γ and $k_d(0)$ of UO_2–DCP unbinding from Mab U08S corresponding to each regression line in Figure 4

		fit 1	fit 2	fit 3	fit 4	fit 5	fit 6	fit 7
Low loading rate†	γ (nm)	0.88 ± 0.30	0.29 ± 0.08	0.15 ± 0.02	0.13 ± 0.04	0.08 ± 0.02	–	–
	$k_d(0)$ (s^{-1})	0.22 ± 0.26	1.67 ± 0.38	1.64 ± 0.12	0.86 ± 0.8	0.4 ± 0.1	–	–
High loading rate	γ (nm)	0.069 ± 0.016	0.023 ± 0.005	0.023 ± 0.002	0.014 ± 0.001	0.013 ± 0.001	0.011 ± 0.001	0.009 ± 0.002
	$k_d(0)$ (s^{-1})	180.7 ± 13.4	43.2 ± 10.9	20.2 ± 3.4	13.6 ± 6.7	8.5 ± 4.8	3.8 ± 0.7	1.4 ± 0.64

*The numbering of fits starts from the bottom line of Figure 4 (in red).
The symbol "–" represents data not observed.

DOI: 10.1002/jmr

Table 2. The results of energy barrier width and dissociation rate constant for both Mabs U08S and U04S systems

Model	Loading rate		Mab U08S	Mab U04S
Bell–Evans	Low	γ	0.08–0.88 nm	0.17–0.90 nm
		$k_d(0)$	0.2–1.7 s^{-1}	0.06–0.12 s^{-1}
	High	γ	0.01–0.07 nm	0.03–0.08 nm
		$k_d(0)$	3.8–181 s^{-1}	0.3–13 s^{-1}
Williams	Low	γ	0.57 nm	0.7 nm
		$k_d(0)$	0.1 s^{-1}	0.14 s^{-1}
	High	γ	0.09 nm	0.19 nm
		$k_d(0)$	0.08 s^{-1}	0.13 s^{-1}

loading rates, and are thus referred to as non-specific interactions. These data points correspond to the fit 1 in the Bell–Evans analysis (Figure 4). Excluding the fit 1, we obtained, at low and high loading rates respectively, the average γ value of 1.6 ± 0.09 and 0.15 ± 0.01 and a range of values for $k_d(0)$ from 0.36 to 1.67 s^{-1} at low loading rates and from 2.2 to 43.2 s^{-1} at high loading rates. As expected the $k_d(0)$ values decrease when the number of parallel bonds increase. Table 2 shows the results for every fit of the Mab U04S and U08S systems. The two systems have similar energy landscapes of unbinding process based on both Bell–Evans and Williams models, though the bond strength between UO_2–DCP and Mab U08S seems weaker according to the Bell–Evans model with a slightly greater $k_d(0)$. Two types of energy barrier width were found for both systems: one with a value greater than 1 Å at low loading rate and the other smaller than 1 Å at high loading rate. This indicates that the unbinding process of UO_2–DCP complexed with antibody goes through two energy barriers; one requires higher energy cost to unbind the metal compound while the other detaches the chelator from the antibody with a longer distance but greater ease.

Analysis of bonding states of multiple parallel-bond systems

Our studies are focused on the bonding between the chelate compound and antibody. However, the measured protein elasticity in our system also includes that observed with protein A which is chemically attached to the gold substrate. Therefore, the influence of protein A needs to be taken into account in determining the loading rate. It appears clearly that refinement is possible if the viscoelastic properties of all molecules involved in the experiment are characterized. In any case, the determination of k_{p1} for n parallel bonds is by no means the only step.

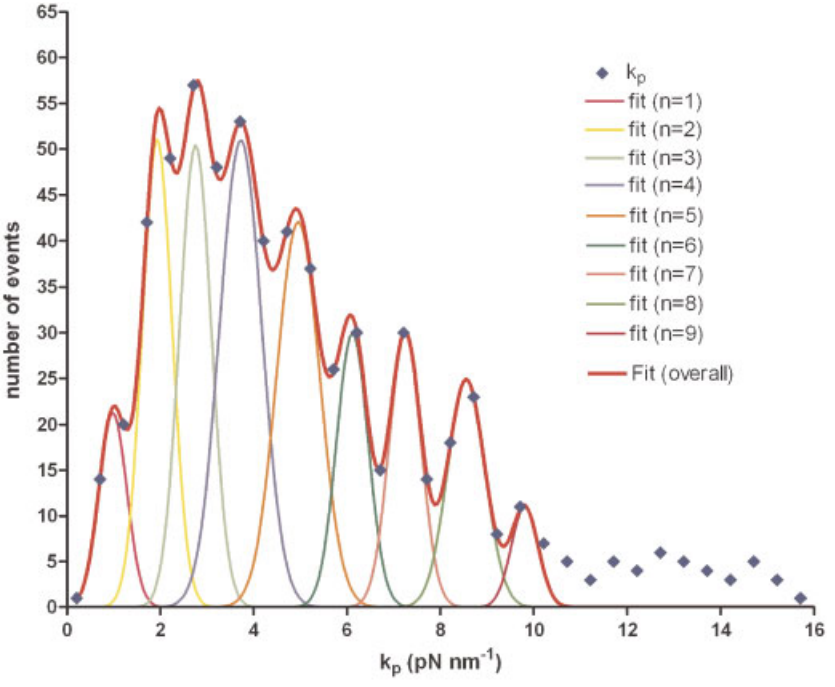

Figure 5. The histogram of unbinding events with respective to k_p for UO_2–DCP bound to Mab U08S. The data labeled by diamonds are experimental results. The red line is composed of Gaussian fits for individual populations corresponding to different bond numbers. Each fit contains an event number greater than 10. This figure is available in colour online at www.interscience.wiley.com/journal/jmr

DOI: 10.1002/jmr

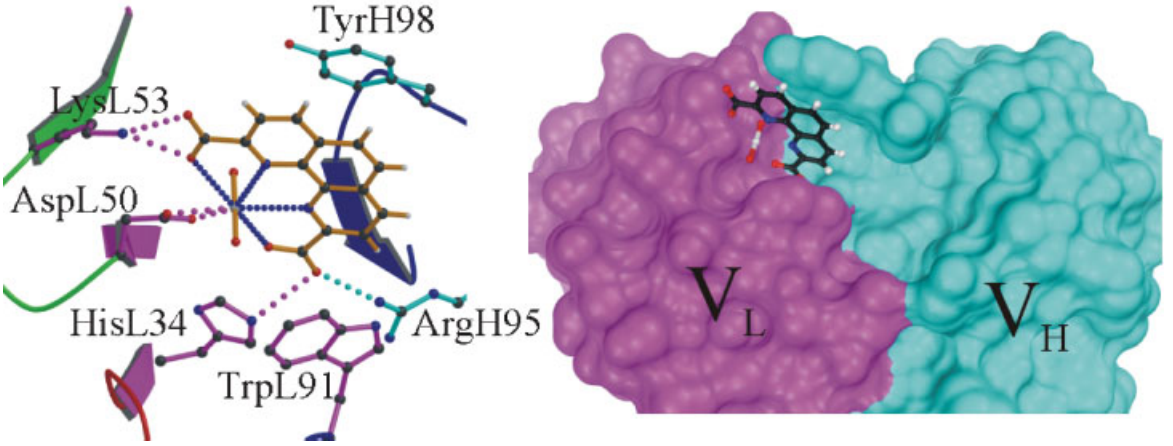

Figure 6. The three-dimensional molecular model of Mab U08S variable fragment. The light chain (V_L) is colored in magenta and the heavy chain (V_H) in cyan. (A) The CDRH3 conformation (red) was remodeled based on the template antibody 1AY1. The uranium atom is chelated with DCP (orange sticks) by navy blue bonds. A bond of chelating coordination is formed between the UO_2^{2+} ion and Mab U08S (magenta and cyan sticks) is formed through the residue AspL50 in CDRL2. In the model, DCP forms hydrogen bonds with HisL34 (CDRL1) and ArgH95 (CDRH3) as well as a salt bridge with LysL53 (CDRL2). The picture was constructed using Molscript (Kraulis, 1991) and rendered by Raster3D (Merritt and Bacon, 1997). (B) The molecular surface of Mab U08S variable fragment. The picture was constructed using the PMV software (Sanner, 1999) to illustrate the shallow binding pocket of Mab U08S for UO_2–DCP (colored balls and sticks).

Recall that $k_p = nk_{p1}$ for n parallel bonds with identical chemical characteristics. We plotted a histogram of k_p for the Mab U08S system which is presented in Figure 5. Assuming that the first peak corresponds to $n = 1$, n was estimated up to 9 from the k_p histogram. The number is in close agreement with that obtained by the Williams model ($n = 8$). In a similar way, we obtained $n \approx 16$ for U04S (data not shown). The discrepancy between the Mab U08S and U04S systems can be explained by the different antibody concentrations that were used. As a result, we obtained values of k_{p1} as 1.00 ± 0.06 pN/nm and 0.87 pN/nm respectively for Mabs U08S and U04S, which are at least five times softer than k_c. In order to investigate the impact of the k_{p1} value upon the kinetic parameters $k_d(0)$ and γ, we tested $k_{p1} = 10$ pN/nm instead of 1 pN/nm to re-calculate $k_d(0)$ and γ. We found that $k_d(0)$ changed by 400% but γ did not change more than 10%. This is expected because k_{p1} is a measure of the binding strength and $k_d(0)$ indicates the efficiency of bond breaking. We have shown that it is possible to obtain the value of n, the number of parallel bonds in a system, by investigating the viscoelasticity of bound molecules on the substrate. A more accurate value of n can be obtained if the stiffness of each molecule is characterized.

A hypothetical mechanism for UO_2–DCP dissociated from the antibody environment

We have built comparative molecular models of UO_2–DCP bound to both Mabs U04S (Odorico *et al*., 2007a) and U08S. In order to position UO_2–DCP into the binding site of the antibody, we have hypothesized that the unfilled coordination site of uranium is occupied by a carboxylic group of Asp or Glu residues in proteins. In Mab U04S, there are only two solvent-accessible Asp residues, while Mab U08S has only one. Although there is one another Asp located at the extremity of CDRH1 in both Mabs U08S and U04S; it was not considered in our structural analysis because of the limited number of interactions that UO_2–DCP can perform in such location of the antibody unless a large conformational change is hypothesized. Because of similar energy landscapes observed in both Mab systems, we suggest that the binding location and coordination mode for UO_2–DCP are likely to be similar in the two Mabs. Accordingly, residue AspL50 present in both Mabs U04S and U08S may play a critical role in chelating with uranium, and model B from our previous work for Mab U04S (Odorico *et al*., 2007a) can also serve as a model for Mab U08S as displayed in Figure 6. It shows that UO_2–DCP is sandwiched between TyrH98 and TrpL91 and that the metal-free chelate DCP forms salt bridges with LysL53 and ArgH95 of the antibody. When combined with the results of the kinetic analysis, this indicates that the UO_2–DCP compound undergoes unbinding from the antibody by a two-step process: first a weakening or breaking of the uranium-AspL50 bond and then a rupturing of the salt bridges between DCP and the antibody. Moreover, the bond strength of uranium-AspL50 is greater than that of salt bridges. Although Mabs U04S and U08S are specific to the uranyl ion, DCP participates in improving the fit of the ion into the binding site of the antibody and consequently helps in stabilizing the whole complex. In conclusion, to design an antibody that efficiently binds the toxic uranium compound, it will be necessary to focus not only on the amino acid constituents in the binding pocket of the antibody but also on the chemical structure of the metal-free chelate.

Acknowledgments

This work has been supported by the program for environmental nuclear toxicology of the Commissariat à l'Énergie Atomique (CEA), France. We gratefully acknowledge Pierre-Henri Puech for critical reading of the manuscript and Marc HV Van Regenmortel for editorial improvements.

DOI: 10.1002/jmr

REFERENCES

Ansoborlo E, Prat O, Moisy P, Den Auwer C, Guilbaud P, Carriere M, Gouget B, Duffield J, Doizi D, Vercouter T, Moulin C, Moulin V. 2006. Actinide speciation in relation to biological processes. *Biochimie* **88**: 1605–1618.

Bell GI. 1978. Models for the specific adhesion of cells to cells. *Science* **200**: 618–627.

Brünger AT. 1992. X-PLOR, version 3.1. A System for X-ray Crystallography and NMR. Yale University Press: New Haven, CT.

Chen S-wW, Pellequer JL. 2004. Identification of functionally important residues in proteins using comparative models. *Curr. Med. Chem.* **11**: 595–605.

Erdmann T. 2005. Stochastic Dynamics of Adhesion Clusters under Force. Theoretische Physik, Universität Potsdam: Potsdam.

Evans E. 2001. Probing the relation between force–lifetime–and chemistry in single molecular bonds. *Annu. Rev. Biophys. Biomol. Struct.* **30**: 105–128.

Evans E, Ritchie K. 1997. Dynamic strength of molecular adhesion bonds. *Biophys. J.* **72**: 1541–1555.

Evans E, Williams P. 2002. Physics of Bio-Molecules and Cells, Vol. **75**: 145–204, Flyvbjerg H, Jülicher F, Ormos P, David F, Eds. Springer–Verlag.

Gorden AE, Xu J, Raymond KN, Durbin P. 2003. Rational design of sequestering agents for plutonium and other actinides. *Chem. Rev.* **103**: 4207–4282.

Kraulis PJ. 1991. MOLSCRIPT: a program to produce both detailed and schematic plots of protein structures. *J. Appl. Cryst.* **24**: 946–950.

Laskowski RA, MacArthur MW, Moss DS, Thornton JM. 1993. PROCHECK: a program to check the stereochemical quality of protein structures. *J. Appl. Cryst.* **26**: 283–291.

MacKerell AD, Bashford D, Bellott M, Dunbrack RL Jr, Evanseck JD, Field MJ, Fisher S, Gao J, Guo H, Ha S, Joseph-McCarthy D, Kuchnir L, Kuczerd K, Lau FTK, Mattos C, Michnick S, Ngo T, Nguyen DT, Prodhom, Reiher WE, III, Roux B, Schlenkrich M, Smith JC, Stote R, Straub J, Watanabe M, Wiorkiewicz-Kuczera J, Yin D, Karplus M. 1998. All-atom empirical potential for molecular modeling and dynamics studies of proteins. *J. Phys. Chem. B* **102**: 3586–3616.

Merritt EA, Bacon DJ. 1997. Raster3D: photorealistic molecular graphics. *Method Enzymol.* **277**: 505–524.

Murali R, Helmer-Citterich M, Sharkey DJ, Scalice ER, Daiss JL, Sullivan MA, Krishna Murthy HM. 1998. Structural studies on an inhibitory antibody against thermus aquaticus DNA polymerase suggest mode of inhibition. *Protein Eng.* **11**: 79–86.

Odorico M, Teulon J-M, Bellanger L, Vidaud C, Bessou T, Chen S-wW, Quéméneur E, Parot P, Pellequer JL. 2007a. Energy landscape of chelated uranyl—antibody interactions by dynamic force spectroscopy. *Biophys. J.* **93**: 645–654.

Odorico M, Teulon J-M, Berthoumieu O, Chen S-wW, Parot P, Pellequer J-L. 2007b. An integrated methodology for data processing in dynamic force spectroscopy of ligand-receptor binding. *Ultramicroscopy* **107***:* 887–894.

Pellequer J-L, Chen S-wW, Keum Y-s, Karu AE, Li QX, Roberts VA. 2005. Structural basis for preferential binding of non-ortho-substituted polychlorinated biphenyls by the monoclonal antibody S2B1. *J. Mol. Recogn.* **18**: 282–294.

Pellequer JL, Zhao B, Kao H-I, Bell CW, Li K, Li QX, Karu AE, Roberts VA. 2000. Stabilization of bound polycyclic aromatic hydrocarbons by a π-cation interaction. *J. Mol. Biol.* **302**: 691–699.

Pible O, Guilbaud P, Pellequer J-L, Vidaud C, Quéméneur E. 2006. Structural insights into protein-uranyl interaction: towards an in-silico detection method. *Biochimie* **88**: 1631–1638.

Sanner MF. 1999. Python: a programming language for software integration and development. *J. Mol. Graph Model* **17**: 57–61.

Sulchek TA, Friddle RW, Langry K, Lau EY, Albrecht H, Ratto TV, Denardo SJ, Colvin ME, Nay A. 2005. Dynamic force spectroscopy of parallel individual Mucin1-antibody bonds. *Proc. Natl. Acad. Sci. USA* **102**: 16638–16643.

Vidaud C, Dedieu A, Basset C, Plantevin S, Dany I, Pible O, Quemeneur E. 2005. Screening of human serum proteins for uranium binding. *Chem. Res. Toxicol.* **18**: 946–953.

Williams PM. 2003. Analytical descriptions of dynamic force spectroscopy: behaviour of multiple connections. *Analyt. Chim. Acta* **479**: 107–115.

DOI: 10.1002/jmr